Fe^{3+}-Doped Anatase TiO_2 Study Prepared by New Sol-Gel Precursors

Bahram Khoshnevisan[1], Mohammad Bagher Marami[1], Majid Farahmandjou[2]**

[1]*Department of Physics, Faculty of Science, University of Kashan, Kashan, Islamic Republic of Iran*
[2]*Departments of Physics, Varamin Pishva Branch, Islamis Azad University, Varamin, Iran*

(Received 4 November 2017)

$Fe_xTi_{1-x}O_2$ (x = 0.00, 0.05, 0.10) nanocomposites are synthesized using a sol-gel method involving an ethanol solvent in the presence of ethylene glycol as the stabilizer, and acetic acid as the chemical reagent. Their structural and optical analyses are studied to reveal their physicochemical properties. Using the x-ray diffractometer (XRD) analysis, the size of the nanoparticles (NPs) is found to be 18–32 nm, where the size of the NPs decreases down to 18 nm when Fe impurity of up to 10% is added, whereas their structure remains unchanged. The results also indicate that the structure of the NPs is tetragonal in the anatase phase. The Fourier transform infrared spectroscopy analysis suggests the presence of a vibration bond (Ti–O) in the sample. The photoluminescence analysis indicates that the diffusion of Fe^{3+} ions into the TiO_2 matrix results in a decreasing electron–hole recombination, and increases the photocatalytic properties, where the best efficiency appears at an impurity of 10%. The UV-diffuse reflection spectroscopy analysis indicates that with the elevation of iron impurity, the band gap value decreases from 3.47 eV for the pure sample to 2.95 eV for the 10 mol% Fe-doped TiO_2 NPs.

PACS: 75.50.Tt, 75.75.Cd, 81.16.−c, 81.07.−b, 73.63.Bd DOI: 10.1088/0256-307X/35/2/027501

In recent years, titanium dioxide (TiO_2) has been used extensively for applications in different industries due to its suitable physicochemical properties. This has been shown in bulk form, or in micro/nano sizes.[1–9] TiO_2 has a tetragonal structure and exhibits different phases including rutile, anatase and brookite. The crystal structure of every phase depends on the way the octahedral blocks are connected in the TiO_2 crystal network.[6] Therefore, each of them shows different properties and applications. Currently, the rutile phase is used as a ferromagnetic material[4] as well as a catalyst in gas sensors,[5] and the anatase phase is employed as an anode in lithium-ion batteries,[7] photocatalysts,[6] filters for ultraviolet waves,[8] production of hydrogen gas,[9] and solar cells.[6]

Due to its chemical stability, lack of toxicity, low price, electric and optical characteristics, and high optical activities (photo activity), titanium dioxide has been used as one of the most common semiconductor photocatalysts.[10–12] Recently, we reported a successful synthesis of TiO_2 NPs using a low price sol-gel method[13] for use in photocatalytic and optoelectronic systems. Apart from the advantages mentioned above, this compound has the following disadvantages: less utilization of photons (less than 4% of sunlight), a relatively high rate of recombination of electrons and holes produced by light, and activity limited to a specific wavelength range (less than 400 nm). Doping TiO_2 with transition metal ions, such as Fe^{3+}, Co^{3+}, Ni^{2+} and Cu^{+}, is one of the modifications for these catalysts to extend the wavelength into the visible region.[14,15] Studies have shown that transition metal elements including Fe^{3+} can be used to enhance photocatalytic activity.[16] The Fe^{3+} metal ions can easily be replaced in the TiO_2 network structure due to its electron configuration. In addition, its ionic radius is close to that of Ti^{4+}, thus it can enhance the photocatalytic properties within the visible light region.[10–12] Therefore, the Fe^{3+} ion has been considered as an effective and considerable doping agent compared with the other transition metals.[17] There are various methods for preparing Fe-doped TiO_2 NPs, which include wet impregnation, co-precipitation, sol-gel, hydrothermal, and other methods.[18–20] Out of these, the sol-gel method has been widely used.[17] In this work, Fe^{3+}-TiO_2 NPs have been synthesized with different percentages of iron impurity using the sol-gel method, and their structural, optical, morphological and photocatalytic properties have been examined using the x-ray diffractometer (XRD), FESEM, EDS, the Fourier transform infrared spectroscopy (FTIR), UV-diffuse reflection spectroscopy (UV-DRS), and photoluminescence (PL) analyses.

Pure and Fe-doped TiO_2 NPs were synthesized using $TiCl_4$ and $FeSO_4{\times}8H_2O$ as new precursors by the sol-gel method. To synthesize pure TiO_2, firstly 10 mL of $TiCl_4$ was dissolved in pure ethanol using a magnetic stirrer at room temperature. After 10 min, 5 mL of acetic acid was added to the solution, and then the temperature was elevated to 70℃. At this temperature, 2 mL of ethylene glycol (EG) stabilizer was added. The solution was completely evaporated, and then dried. The powder thus obtained was washed with distilled water and ethanol several times to remove the impurities in the sample. Eventually, the product was incubated at 600℃ for 4 h to form a crystal structure. For fabricating an impure sample, a method similar to the one used for the preparation of the pure TiO_2 sample was adopted. Firstly, the $FeSO_4.8H_2O$ iron precursor was dissolved in pure water to obtain a 1 M solution. It was then added to the $TiCl_4$ solution in ethanol with 5% and 10% molar

**Corresponding author. Email: farahmandjou@iauvaramin.ac.ir

percentages. Similarly, it was allowed to dry at 70℃ to obtain a powder. The solution pH was adjusted to 3 with an acetic acid reagent.

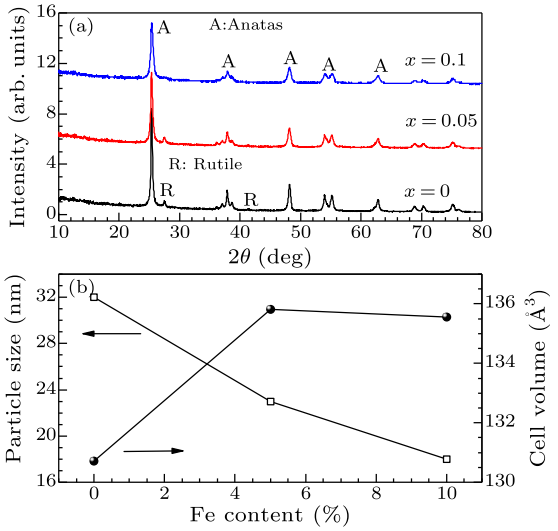

Fig. 1. (a) Compared XRD spectra of pure and Fe-doped TiO_2 nanocrystals for different Fe concentrations. (b) Variation of crystal size and unit cell volume versus Fe dopant.

XRD analysis was carried out to determine the crystal structure, the phases in the sample, and the lattice parameters of the pure and Fe-doped TiO_2 NPs. All the samples were incubated at 600℃ for 4 h, and then were analyzed. Eventually, their crystal structures in the pure and impure states of Fe (including 5% and 10% molar percentages) were examined. The results indicated that the pure sample of TiO_2 had a tetragonal structure with a mixed anatase phase, and some percentage of the rutile phase (8.4%). For the samples with impurity percentages of 5% and 10%, the rutile phase decreased by up to 5.7% and 2.25%, respectively, and the samples almost entered the anatase phase. The results also showed that in spite of the iron impurities within the TiO_2 structure, the structure remains unchanged (with slight changes in the lattice constants), signifying that the iron impurity does not influence the TiO_2 matrix. Figure 1(a) reveals the XRD spectra of the pure and impure samples of Fe. As shown in the figure, the major peaks of the anatase phase at a 2θ angle emerge at 25.37, 37, 37.85, 38.62, 48.11, 53.94, 55.12, 62, 72, 68.84, 70.33, 75.09 and 76.13, which correspond to the crystal planes of (101), (103), (004), (112), (200), (105), (211), (118), (116), (220), (125) and (031), respectively. This suggests that the anatase phase has a tetragonal structure. Further, the weak peaks emerge at 2θ angles of 27.49, and 41.30, corresponding to (110) and (210) crystal planes, respectively, suggesting that the rutile phase occurs in the pure TiO_2 sample. By applying 10% Fe impurity, the rutile level diminishes, and the sample changes into the anatase phase. It can also be obtained that the ionic radii of Fe^{3+} and Ti^{4+} are very close to each other ($a_{Fe}^{3+} = 0.64$ Å, and $a_{Ti}^{4+} = 0.68$ Å), thus Fe^{3+} ions can easily replace the Ti^{4+} ions in the TiO_2 crystal structure, resulting in a constancy of the TiO_2 structure. The particle size for pure and Fe-doped TiO_2 samples was calculated using the Debye–Scherrer formula.[21] Figure 1(b) indicates the changes in the size of the NPs in terms of the impurity percentage of Fe. The size of the pure TiO_2 NPs is 32 nm, and the sizes of the impure $Fe_xTi_{1-x}O_2$ NPs have been measured to be 23 and 18 nm for $x = 0.05$ and $x = 0.10$, respectively. In addition, as the ionic radius of Fe^{3+} is smaller than that of Ti^{4+}, with the entrance of the Fe^{3+} ions into the TiO_2 matrix, the particle size decreases. In Fig. 1(b), the unit cell volume also increases with the elevation of impurity by up to 5%, whereas it is almost constant for 10% impurity. The elevation of the impurity percentage increases the unit cell volume due to an over-aggregation of the iron atoms in the TiO_2 network structure, and increases the lattice constant of network a.

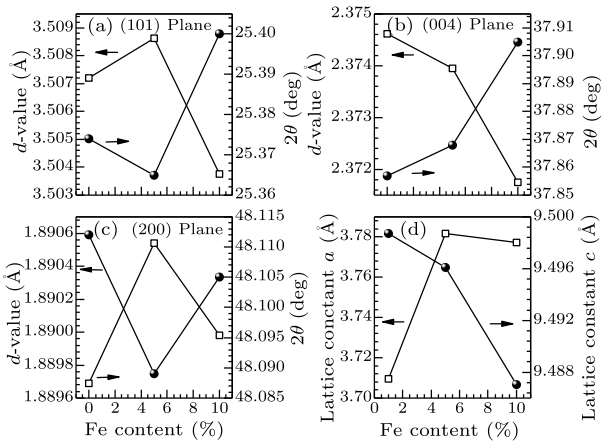

Fig. 2. Plot of diffraction peak of Fe-doped TiO_2 (a) $d(101)$, $2\theta(101)$; (b) $d(004)$, $2\theta(004)$; and (c) $d(200)$, $2\theta(200)$. (d) Lattice parameters a and c versus Fe dopant (mol%).

Figure 2 reveals the changes in the lattice parameters in terms of the iron impurity percentage. As can be seen from the analysis, an elevation of the impurity percentage of up to 5% leads to an increase in the distance between (101) and (200) planes, whereas along (400), this distance decreases (Figs. 2(a)–2(c)). Indeed, the Fe^{3+} atoms have replaced the Ti^{4+} ions in the TiO_2 matrix, mostly in the aforementioned crystal direction. Further, as they have a smaller ionic radius, the distance between the planes within this direction declines. In addition, increasing the iron impurity by up to 10% causes the distance between the planes to decrease due to the over-aggregation of iron atoms in the TiO_2 matrix, which has the maximum percentage of the anatase phase in the crystal structure. An alteration of the 2θ angle causes the planes of (100) and (200) to incline towards smaller angles with the elevation of the impurity percentage up to 5%, whereas the plane of (004) inclines towards larger angles. The reason for these changes is due to the phenomenon that all Fe^{3+} ions cannot be replaced in the TiO_2 ma-

trix completely, and hence, a distortion is developed at the 2θ angle sites in these crystal planes. Figure 2(d) represents the changes in the lattice constants of a and c in terms of the iron impurity percentage. Evidently, the elevation of iron impurity causes the lattice constant a to increase. On the other hand, the lattice constant c decreases, which corresponds to the changes in the distance between the (200) and (004) planes. Indeed, the very trivial difference in the ionic radii of Fe^{3+} and Ti^{4+} (around 0.04 Å) results in a diminished lattice constant c. The changes in the lattice parameters for the different iron impurity percentages are listed in Table 1. The alterations of particle size, unit cell volume, particle volume, the number of unit cells in each particle, band gap energy, and FWHM with variations in the iron impurity percentage have been listed in Table 2.

Table 1. Lattice parameters and Bragg angles (2θ) of pure and Fe-doped TiO_2 nanocrystals.

Fe dopant (mol%)	2θ(deg) (101)	d (Å) (101)	2θ(deg) (200)	d (Å) (200)	2θ(deg) (004)	d (Å) (004)	$a=b$ (Å)	c (Å)	c/a
JCPDS	25.304	3.51685	48.037	1.89250	37.797	2.37825	3.7850	9.5130	2.51334
Pure	25.374	3.50721	48.112	1.88969	37.857	2.37462	3.70942	9.49873	2.5607
5	25.365	3.50863	48.089	1.89054	37.868	2.37395	3.78181	9.4961	2.51099
10	25.4	3.50375	48.105	1.88998	37.905	2.37175	3.77736	9.48703	2.51155

Table 2. FWHM, particle size, volume of the NPs, volume of the unit cell, number of unit cells, band gap energy and lattice strain of pure and Fe-doped TiO_2 samples.

Fe dopant (mol%)	FWHM	D Particle size (nm)	V NPs Volume (nm^3)	v Tetragonal unit-cell volume ($10^{-3}nm^3$)	V/v Number of unit cell per particle (10^3)	Band gap energy (eV)	Lattice strain ξ along the a-axis (10^{-4})
Pure	0.335	32	17148	130.7006	131.2	3.47	20
5	0.347	23	6367	135.814	46.9	3.30	20
10	0.441	18	3052	135.5652	32.5	2.95	28

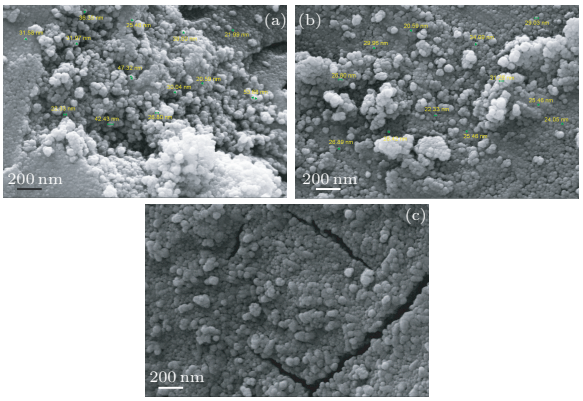

Fig. 3. FESEM images of (a) pure, (b) 5% and (c) 10% Fe-doped TiO_2.

The appearance and mean diameter of the NPs were analyzed by a field emission scanning electron microscope (FESEM). As shown in Fig. 3, elevation of the iron impurity decreases the homogeneity of the Fe-doped TiO_2 NPs in comparison with pure TiO_2, which is due to the reduction of the particle size. Evidently, with the reduction of size of the particles, interatomic attraction and molecular forces grow, thereby the tendency of the NPs is enhanced to approach each other, which causes agglomeration.[22] Figure 3(a) shows the pure TiO_2 NPs with a mean size of 33 nm, and Figs. 3(b) and 3(c) reveal TiO_2 NPs with iron impurity of 5% and 10% with a mean size of 24 nm and 20 nm, respectively, which are in congruence with the results of the XRD analysis.

The EDX analysis has been used to determine the elemental percentage in the sample. Figure 4 demonstrates the x-ray energy diffraction spectrum for iron impurity of 5%. Clearly, only O, Ti and Fe elements exist in the sample, indicating the purity of the sample. In the sample, the weight percentage of iron has been measured as 2.3%, which is less than the 5% molar percentage used in the experiment. This difference in the percentages is due to the fact that in the EDX analysis, the surface of the sample is analyzed and scanned, whereas during the fabrication of the sample, the molar percentage is calculated per sample volume.

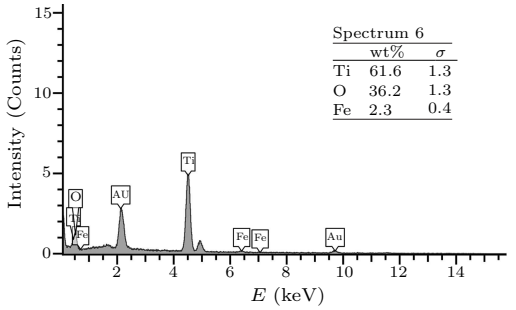

Fig. 4. EDX analysis of 5 mol% of Fe-doped TiO_2 samples. The inset shows the image of Fe-doped TiO_2 NPs.

The TEM analysis of Fe-doped TiO_2 with a 5% level of impurity is displayed in Fig. 5. The TEM study confirms that the particle's size varies in the range 18–28 nm. Uniformity of the particles is desirable and the average size of particles fitting the Gaussian function is about 23.12 nm. According to XRD and FESEM analyses, the average sizes of the particles are measured to be 23 nm and 24 nm, respectively.

The FTIR analysis (within 400–4000 cm^{-1}) has been used to identify the bonds in the sample. Figure

6 shows the FTIR on the sample in terms of wavenumber. The absorption peaks developed in the spectrum represent the existence of vibration bonds in the sample. The comparison of the spectrum of the pure TiO_2 sample and the 5% impurity sample demonstrates that when the iron impurity is incorporated into the TiO_2 matrix, an absorption peak emerges at the wavenumber of 2992 cm^{-1}, which belongs to the O–H vibration bond. The sharp absorption peak at 440 cm^{-1} is attributed to the TiO_2 sample, and the one developed at 465 cm^{-1} is for the 5% impure sample, which is associated with the Ti–O group. Within 650–1800 cm^{-1}, a very sharp peak is developed due to the entrance of environmental oxygen in the sample during the synthesis and fabrication of the NPs.

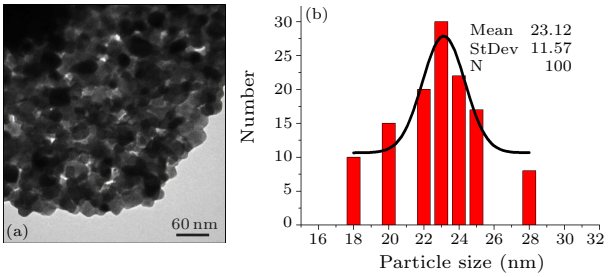

Fig. 5. (a) TEM analysis of 5 mol% of Fe-doped TiO_2 samples. (b) Size distribution of the samples, fitted with the Gaussian curve.

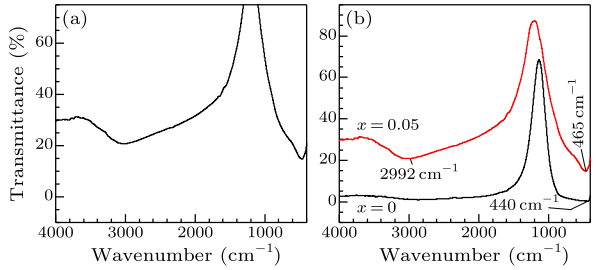

Fig. 6. FTIR spectrum of the Fe-doped TiO_2 nanocomposite for different Fe dopants.

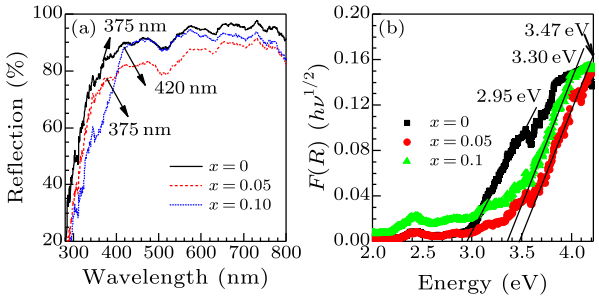

Fig. 7. (a) Reflection spectrum of the Fe-doped TiO_2 samples. (b) Plot of $[F(R)h\nu]^{1/2}$ versus $E(h\nu)$ with different Fe contents.

Figure 7(a) represents the UV reflective spectrum within the wavelengths of 280–300 nm. To determine the absorption wavelength and bandgap energy (E_g) of the sample, the UV-DRS optical analysis has been used. The analysis shows that as the impurity increases, the maximum wavelengths (λ_{edge}) are attained at 357, 375 and 420 nm, for the $x = 0$, $x = 0.05$ and $x = 0.10$ samples, respectively. This reduction in the λ_{edge} observed as the impurity percentage increases leads to the development of a redshift, and consequently, a diminished bandgap energy.

For calculating E_g of the samples, the Tauc plot $(F(R)h\nu)^{1/2}$ has been plotted in terms of the photon energy $E(h\nu)$, where $F(R)$ is the Kubelka–Munk function, and R is the percentage.[23] Figure 7(b) represents the Tauc curve in terms of the iron impurity. The maximum slope of the line tangential to the curve, and its intersection with the energy axis give the bandgap energy value. The results show that as the percentage of impurity increases, the bandgap energy diminishes, such that its values are obtained to be 3.47, 3.30 and 2.95 eV for the $x = 0.00$, $x = 0.05$ and $x = 0.10$ samples, respectively. Moreover, factors such as the size of the impure particles, defects in the lattice, and alteration of the lattice parameters influence the value of the bandgap energy.[24] Researchers have also reported that a reduction of E_g is a result of the sp–d exchange in the interaction between the band electrons of TiO_2 and d electrons of the Fe^{3+} impurity bands.[24]

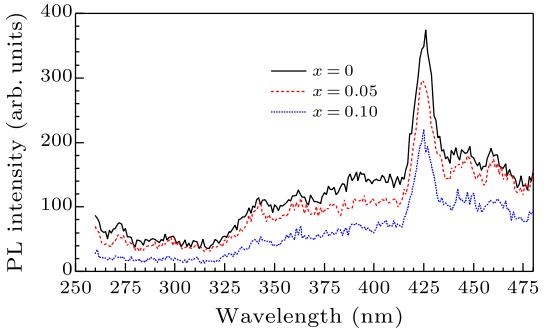

Fig. 8. Photoluminescence spectroscopy of Fe-doped TiO_2 samples for different levels of Fe dopant.

Figure 8 reveals the photoluminescence spectrum of the $Fe_xTi_{1-x}O_2$ sample. To determine the recombination of the sample due to the behavior of the electron–hole pair, the PL optical analysis has been used. As shown in Fig. 8, as the impurity of Fe increases, the intensity of photoluminescence decreases, suggesting that the extent of recombination of the induced electron–hole pairs diminishes, and thus the photocatalytic property of the sample grows. Some peaks are developed at the wavelengths of 342, 363, 376, 390, 425, 447 and 495 nm, which correspond to the energy bandgaps of 3.62, 3.41, 3.29, 3.18, 2.91, 2.77 and 2.70 eV, respectively. Moreover, with the addition of Fe^{3+} impurity, entrapment of the holes by the Ti^{4+} band in the conduction band is prevented by developing the iron impurity level in the bottom of the conduction band, thereby preventing recombination of the electrons and holes. Accordingly, the pairing of electrons and holes in the bottom of the conduction band in the Fe impurity level occurs, causing dimin-

ished intensity of PL, and thus leads to the reduced bandgap energy.[25]

In conclusion, Fe-doped TiO_2 NPs have been successfully synthesized using the sol-gel method. The XRD results indicate that in pure TiO_2 NPs, there is a minor percentage of the rutile phase, whereas with the addition of Fe impurity by up to 10%, a tetragonal structure emerges in the anatase phase. Furthermore, the size of the nanocrystals decreases with the addition of iron impurity by up to 18 nm, without any change in the crystal structure. The PL optical analysis shows that with elevation of impurity percentage by up to 10%, the photoluminescence intensity decreases, causing a reduction of the recombination of electrons and holes, and elevation of the photocatalytic activity. Eventually, the UV-DRS optical analysis shows that with increasing the iron impurity percentage, the maximum wavelength inclines towards larger wavelengths, whereby a redshift state is reached, causing the reduction of bandgap energy by up to 2.95 eV.

References

[1] Pfaff G and Reynders P 1999 *Chem. Rev.* **99** 1963
[2] Bin Q, Wu L, Zhang Y, Zeng Q and Zhi J 2010 *J. Colloid Interface Sci.* **345** 181
[3] Brown W D and Granneman W W 1978 *Solid-State Electron.* **21** 837
[4] Matsumoto Y, Murakami M, Shono T, Hasegawa T, Fukumura T, Kawasaki M, Ahmet P, Chikyow T, Koshihara S and Koinuma H 2001 *Science* **291** 854
[5] Kumazawa N, Islam M R and Takeuchi M 1999 *J. Electrochem. Chem.* **472** 137
[6] Carp O, Huisman C L and Reller A 2004 *Prog. Solid State Chem.* **32** 33
[7] Kavan L, Fattakhova D and Krtil P 1999 *J. Electrochem. Soc.* **146** 1375
[8] Bonini N, Carotta M C, Chiorino A, Guidi V, Malagù C, Martinelli G, Paglialonga L and Sacerdoti M 2000 *Sens. Actuators* B **68** 274
[9] Boccuzzi F, Chiorino A, Manzoli M, Andreeva D, Tabakova T, Ilieva L and Iadakiev V 2002 *Catal. Today* **75** 169
[10] Foura G, Chouchou N, Soualah A, Kouachi K, Guidotti M and Robert D 2017 *Catalysts* **7** 344
[11] Wang F, Shen T, Fu Z, Lu Y and Chen C 2018 *Nanotechnology* **29** 035702
[12] Ali T, Tripathi P, Azam A, Raza R, Ahmed A S, Ahmed A and Muneer M 2017 *Mater. Res. Express* **4** 015022
[13] Ramazani M, Farahmandjou M and Firoozabadi T P 2015 *Phys. Chem. Res.* **3** 293
[14] Pulsipher D I, Martin I T and Fisher E R 2010 *ACS Appl. Mater. Interfaces* **2** 1743
[15] Izmajlowicz M A T, Flewitt A J, Milne W I and Morrison N A 2003 *J. Appl. Phys.* **94** 7535
[16] Xu J P et al 2009 *Chin. Phys. Lett.* **26** 097502
[17] Hu X, An T, Zhang M, Sheng G and Fu J 2007 *Res. J. Chem. Environ.* **11** 13
[18] Ali T, Tripathi P, Azam A, Raza W, Ahmed A S, Ahmed A and Muneer M 2017 *Mater. Res. Express* **4** 015022
[19] Yang Y, Yu Y, Wang J, Zheng W and Cao Y 2017 *Cryst. Eng. Commun.* **19** 1100
[20] Ramalingam R J, Arunachalam P, Radhika T, Anju K R, Nimitha K C and Al-Lohedan C H 2017 *Int. J. Electrochem. Sci.* **12** 797
[21] Scherrer P 1918 *Göttinger Nachr. Gesell.* **2** 98
[22] Chen Q, Xue C, Li X and Wang Y 2013 *Mater. Sci. Forum* **743** 367
[23] Khatoon S, Wani I A, Ahmed J, Magdaleno T, Al-Hartomy O A and Ahmad T 2013 *Mater. Chem. Phys.* **138** 519
[24] Siripala W and Tomkieviez M 1982 *J. Electrochem. Soc.* **129** 1240
[25] Beydoun D, Amal R, Low G and McEvoy S 1999 *J. Nanopart. Res.* **1** 439